THE JOURNAL OF BIOLOGICAL CHEMISTRY VOL. 288, NO. 3, pp. 1896–1906, January 18, 2013

Proinsulin Intermolecular Interactions during Secretory Trafficking in Pancreatic β Cells*

Received for publication, September 17, 2012, and in revised form, December 4, 2012 Published, JBC Papers in Press, December 7, 2012, DOI 10.1074/jbc.M112.420018

Leena Haataja[‡], Erik Snapp[§], Jordan Wright[‡], Ming Liu[‡], Alexandre B. Hardy[¶], Michael B. Wheeler[¶], Michele L. Markwardt[‖], Mark Rizzo[‖], and Peter Arvan[‡1]

From the [‡]Division of Metabolism, Endocrinology, and Diabetes, University of Michigan Medical School, Ann Arbor, Michigan 48105, the [§]Department of Anatomy and Structural Biology, Albert Einstein College of Medicine, Bronx, New York 10461, the [¶]Department of Physiology, University of Toronto, Ontario, Canada M5S 1A8, and the [‖]Department of Physiology, University of Maryland, Baltimore, Maryland 21201

Background: Proinsulin assembly is linked to its intracellular transport.
Results: Proinsulin self-associates in the endoplasmic reticulum but, surprisingly, accumulates at a rate-limiting transport step in the Golgi region.
Conclusion: Proinsulin transport is a dynamic process, and its perturbation may be measured under steady-state conditions.
Significance: Proinsulin distribution may be a useful tool to characterize proinsulin trafficking in disease states.

Classically, exit from the endoplasmic reticulum (ER) is rate-limiting for secretory protein trafficking because protein folding/assembly occurs there. In this study, we have exploited "hPro-CpepSfGFP," a human proinsulin bearing "superfolder" green fluorescent C-peptide expressed in pancreatic β cells where it is processed to human insulin and CpepSfGFP. Remarkably, steady-state accumulation of hPro-CpepSfGFP and endogenous proinsulin is in the Golgi region, as if final stages of protein folding/assembly were occurring there. The Golgi regional distribution of proinsulin is dynamic, influenced by fasting/refeeding, and increased with β cell zinc deficiency. However, coexpression of ER-entrapped mutant proinsulin-C(A7)Y shifts the steady-state distribution of wild-type proinsulin to the ER. Endogenous proinsulin coprecipitates with hPro-CpepSfGFP and even more so with hProC(A7)Y-CpepSfGFP. Using Cerulean and Venus-tagged proinsulins, we find that both WT-WT and WT-mutant proinsulin pairs exhibit FRET. The data demonstrate that wild-type proinsulin dimerizes within the ER but accumulates at a poorly recognized slow step within the Golgi region, reflecting either slow kinetics of proinsulin hexamerization, steps in formation of nascent secretory granules, or other unknown molecular events. However, in the presence of ongoing misfolding of a subpopulation of proinsulin in β cells, the rate-limiting step in transport of the remaining proinsulin shifts to the ER.

In pancreatic β cells, proinsulin is processed to insulin within secretory/storage granules (1). Classically, it is thought that, other than long-term storage in mature secretory granules, steps leading up to exit from the endoplasmic reticulum (ER),[2] typically including protein assembly/oligomerization, are rate-limiting for overall protein trafficking through the secretory pathway (2). Conditions that adversely affect ER export of proinsulin, including dysregulated mRNA translation, impaired ER-to-Golgi traffic (3, 4), or alteration of the ER environment that impairs rate/efficiency of proinsulin monomer folding (5, 6) promote insulin deficiency and glucose intolerance. Conversely, enhanced exit from the ER is correlated with increased protein entry into forming granules, (7) which, in β cells, increases insulin production (8). These findings seem to imply that proinsulin egress from the ER is rate-limiting for insulin production. If so, then, at steady state, accumulation of proinsulin molecules should be detectable at or just before this rate-limiting step. Certainly, point mutations within proinsulin greatly exaggerate the ER residence time of proinsulin (9). However, given the critical importance of secretory protein assembly/oligomerization in protein trafficking (10–13), it is surprising how little we know about proinsulin assembly in relation to its intracellular transport.

Insulin can form crystalline inclusions in secretory granules (14). The basic unit of the insulin crystal is a hexamer (15). In β cells, proinsulin hexamerization is facilitated by the presence of zinc ions (16) catalyzed by zinc transport via ZnT8 that is contained in the Golgi complex (17, 18). Although the intracellular site(s) of proinsulin assembly remain unproved, hexamer formation in the Golgi complex is hypothesized (19).

Association of proinsulin monomers should be testable with the advent of proinsulins engineered to contain variants of GFP embedded within the proinsulin connecting (C)-peptide (20–23). However, some GFP variants can exhibit impaired folding in the oxidizing environment of the ER (24), which could affect

* This work was supported, in whole or in part, by National Institutes of Health Grants R01-DK48280 (to P. A.), R01-DK077140 (to M. A. R.), R01-GM086530 (to E. S.), R01-DK088856 (to M. L), and CIHR MOP-102588 (to M. B. W.).
[1] To whom correspondence should be addressed: Division of Metabolism, Endocrinology, and Diabetes. University of Michigan, 5112 Brehm Center,1000 Wall St., Ann Arbor, MI 48105-51714. Tel.: 734-936-5505; Fax: 734-936-6684; E-mail: parvan@umich.edu.

[2] The abbreviations used are: ER, endoplasmic reticulum; hPro, human proinsulin; Cpep, connecting peptide; CFP, cyan fluorescent protein; ER-RFP, ER-red fluorescent protein; KDEL, Lysine, Aspartic acid, Glutamic acid, Leucine; NA, Numerical Aperture; RIA, radioimmunoassay; RIP, rat insulin promoter; SfGFP, superfolder GFP; GRINCH, glucose-responsive, insulin-secreting, c-peptide-modified human proinsulin.

both rate and efficiency of chimeric proinsulin export. The eight "superfolder" (Sf) substitutions improve the kinetics and efficiency of GFP folding (25) and prevent formation of disulfide-linked GFP oligomers, creating a new tool for studying secretory protein trafficking (26). Here we have exploited the hPro-CpepSfGFP, hPro-CpepSfVenus, and hPro-CpepSfCerulean constructs to examine the site of steady-state accumulation and the first direct examination of proinsulin assembly within the secretory pathway in pancreatic β cells.

EXPERIMENTAL PROCEDURES

Cell Culture—U2OS cells (26) and INS1 and INS 832/13 β cells were cultured as described (27, 28). COS7 cells were cultured in DMEM containing L-glutamine, 10% FBS, and penicillin-streptomycin.

Plasmids—cDNAs encoding SfGFP (25), SfCerulean (29), and SfVenus (30) were amplified and ligated into the ApaI site (*In-Fusion*, Clontech) located within the C-peptide coding sequence (21) to make hPro-CpepSfGFP, hPro-CpepSfCerulean, and hPro-CpepSfVenus. The "*Akita*-like" proinsulin C(A7)Y and addition of encoded C-terminal KDEL sequence mutations were introduced (QuikChange, Stratagene). ER-RFP was described previously (31). All cDNAs were verified by direct DNA sequencing.

Transfection—INS1 cells were transfected with Lipofectamine 2000 (Invitrogen). 48 h post-transfection, cells were lysed in boiling SDS gel sample buffer. For stable transformants, growth medium containing 0.2 mg/ml G418 was used, and 12 distinct colonies bearing hPro-CpepSfGFP were expanded. All experiments in this study used GRINCH clone 8. For cells bearing hProC(A7)Y-CpepSfGFP, stable transformants were a pooled population of G418-resistant cells.

Western Blotting—Proteins were resolved (4–12% NuPAGE Bis-Tris gels, 10 μg/lane, Invitrogen), electrotransferred to nitrocellulose, and immunoblotted with guinea pig anti-insulin (Linco/Millipore), rabbit anti-GFP (Immunology Consultants) or mouse anti-tubulin (Sigma). Horseradish peroxidase-conjugated secondary antibodies were from Jackson ImmunoResearch Laboratories, Inc., with proteins visualized by ECL (Millipore).

Glucose-stimulated Insulin Secretion—Cells (in 24 wells) grown to confluency underwent medium change to 5 mM glucose 18 h before preincubation for 2 h in Krebs-Ringer's-bicarbonate-Hepes containing 0.5% bovine serum albumin and 2.8 mM glucose. After preincubation, cells were incubated for 1 h in the same buffer ("basal") followed by 1 h incubation in Krebs-Ringer's-bicarbonate-Hepes with 16.7 mM glucose ("stimulated"). Media were collected, and cells were lysed in boiling SDS gel sample buffer. For overnight insulin secretion, regular medium containing 11 mM glucose was changed to fresh medium and collected for 18 h. Insulin was measured (normalized to cell protein) by rat insulin radioimmunoassay (RIA) (cross-reacting between species and with proinsulin) or human insulin- or proinsulin-specific RIAs (Millipore).

Metabolic Labeling— 48 h post-transfection, cells were incubated for 0.5 h in RPMI 1640 medium lacking Cys/Met and then labeled for 0.5 h in the same medium containing ^{35}S-amino acids (MP Biomedicals). Cells were chased in complete RPMI at 2.8 or 11 mM glucose or were stimulated as described (27). Cells were lysed in 25 mM Tris (pH 7.5), 1% Triton X-100, 0.2% deoxycholic acid, 0.1% SDS, 10 mM EDTA, 100 mM NaCl, and a protease inhibitor mixture (Roche).

Immunoprecipitation—Cell lysates and chase media were precleared (Zysorbin, Invitrogen) and immunoprecipitated overnight with anti-GFP or anti-insulin and protein A-agarose. To reimmunoprecipitate insulin from GFP immunoprecipitates, beads were boiled in 1% SDS, diluted in lysis buffer lacking SDS, and immunoprecipitated with anti-insulin. Immunoprecipitates were analyzed by reducing 4–12% NuPAGE with phosphorimaging.

Confocal Imaging of GRINCH and INS1 Cells—GRINCH or INS1 cells plated on chamber slides (Nalge-Nunc) were untransfected or transfected. In Fig. 4*B*, regular medium was replaced with low (2.8 mM) glucose- or high (16.7 mM) glucose-containing medium for 4 h. In all experiments, cells were fixed in 3.7% formaldehyde in PBS (pH 7.4) for 20 min at room temperature, washed with PBS, permeabilized with 0.4% Triton X-100 in TBS, blocked with TBS containing 3% BSA and 0.2% Triton X-100, and then stained overnight (4 °C) with primary antibodies (guinea pig anti-insulin (Dako), mouse anti-proinsulin (ALPCO), mouse anti-GM130 or Alexa Fluor 555-conjugated mouse anti-GM130 (BD Biosciences), or rabbit anti-calnexin or rabbit anti-membrin (Enzo Life Sciences)) diluted in TBS containing 3% BSA and 0.2% Tween 20. Thereafter, sections were rinsed and incubated with secondary antibodies conjugated to Alexa Fluor 488, 555, or 647 (Invitrogen). Slides were mounted with Prolong Gold with DAPI (Invitrogen) and imaged by epifluorescence in an Olympus FV500 confocal microscope with ×60 (Numerical Aperture (NA) 1.4) or ×100 (NA 1.35) oil objectives.

Immunofluorescence of Transiently Transfected Cells—Overnight-transfected U2OS or INS1 cells were fixed for 15 min as above, permeabilized with 0.1% Triton X-100 in PBS, and blocked with 10% FBS in PBS. Cells were labeled with mAb anti-p115 (from Dr. D. Shields, AECOM, NY) followed by Alexa Fluor 555-conjugated anti-mouse IgG. Cells were imaged under laser illumination with a Duoscan confocal microscope (Zeiss) with a ×60 (NA 1.4) oil objective.

Mouse Pancreas Immunofluorescence—Pancreata from 3-month-old C57BL/6J mice fasted overnight and then refed for 6 h or from randomly fed Ins2-Cre ("RIP-Cre") or ZnT8BKO (β cell-specific ZnT8 knockout) mice were prepared as described (32) and cut into 5-μm paraffin sections. Sections were deparaffinized in Citrisolv (Fisher); rehydrated in a graded series of alcohols; washed in H_20 followed by antigen retrieval (Retrieve-ALL-1, Covance); and immunostained with mouse anti-proinsulin 1:500, rabbit anti-GM130 1:200 (catalog no. ab52649, Abcam), mouse anti-GM130 1:500, or rabbit anti-calnexin 1:200 and guinea pig anti-insulin 1:500. Secondary antibodies were conjugated to Alexa Fluor 488, 555, or 647. With an average of 840 insulin-positive β cells (10 islets), the proinsulin-positive Golgi area was compared between genotypes by creating a thresholded binary mask defining the GM130-positive area superimposed on the proinsulin-positive area (Metamorph 7.7.7, Molecular Devices) to calculate the Golgi proinsulin area/β cell.

Anisotropy FRET Microscopy—Cells (on 35-mm glass bottom dishes, Mat-Tek) were transfected using LipoD293 (Signa-

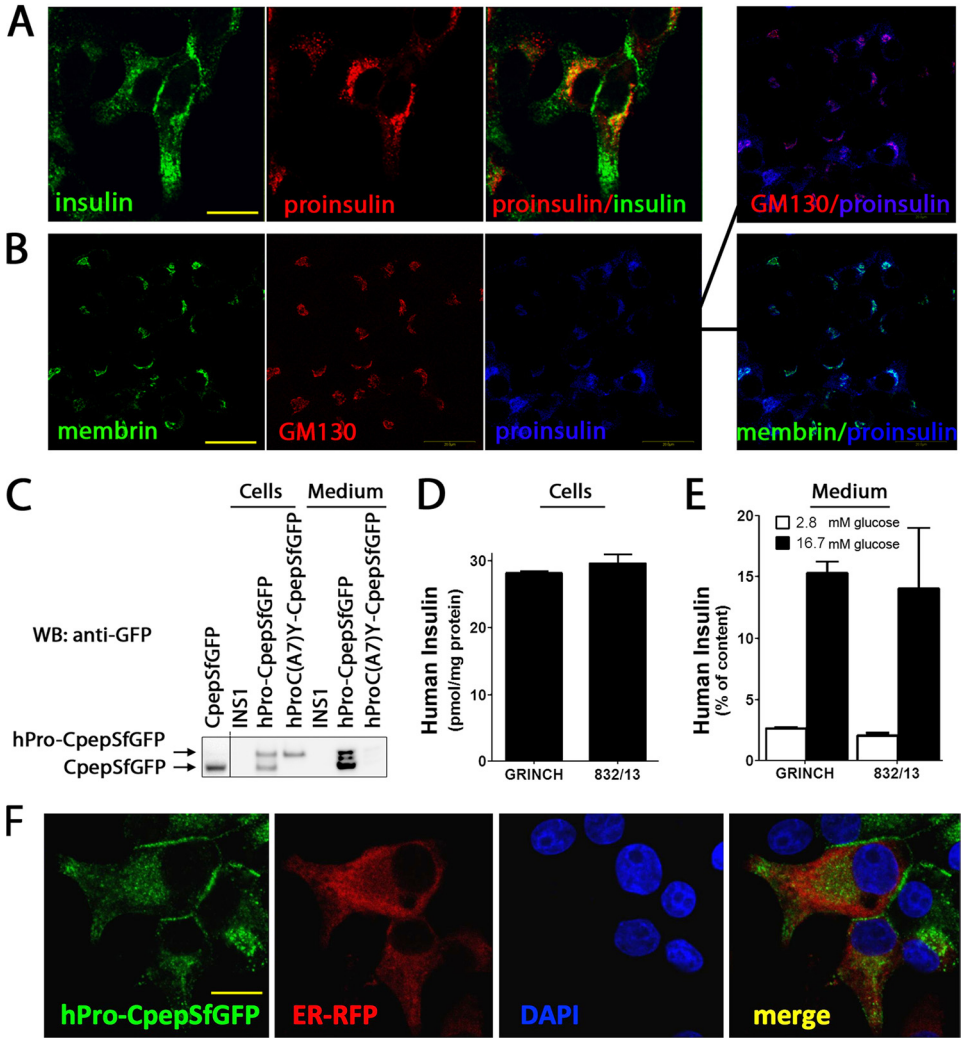

FIGURE 1. **Expression of endogenous proinsulin and hPro-CpepSfGFP in INS1 cells.** *A*, parental INS1 cells were processed for double-label immunofluorescence with guinea pig anti-insulin that cross-reacts with proinsulin (*green*) and mouse mAb anti-proinsulin that does not cross-react with insulin (*red*; a *merged* image is also shown, right *panel*). Confocal microscopy, *scale bar* = 10 μm. *B*, parental INS1 cells were processed for triple-label immunofluorescence with rabbit polyclonal anti-membrin (an ER-to-Golgi SNARE protein, *green*), Alexa Fluor 555-conjugated mouse anti-GM130 (a Golgi matrix protein, *red*), and a mouse mAb anti-proinsulin that does not cross-react with insulin (*blue*). A merged pairwise image is also shown (*right panel*). *Scale bar* = 20 μm. *C*, parental INS1 cells or GRINCH cells (INS1 cells stably expressing hPro-CpepSfGFP) or INS cells expressing hProC(A7)Y-CpepSfGFP were plated in 12-well plates. The bathing media were collected after 18 h, and the cells were lysed. All samples were then resolved by reducing SDS-PAGE in 4–12% acrylamide gradient gels and electrotransfer to nitrocellulose for direct immunoblotting (*WB*) with anti-GFP. Note that hPro-CpepSfGFP shows processing to CpepSfGFP (a recombinant CpepSfGFP standard is shown at the *left*) as well as extensive secretion. Human insulin content (*D*) and insulin secretion (*E*) after unstimulated (2.8 mM glucose, *open bars*) and stimulated (16.7 mM glucose, *closed bars*) collections from GRINCH and INS832/13 (*832/13*) cells. Human insulin RIA is specific for processed, mature, human insulin, and this comprises 6–8% of total proinsulin + insulin of all species in GRINCH and 832/13 cells. Data from three independent measurements are shown. Data are mean ± S.D. *F*, GRINCH cells were transiently transfected to express an ER-targeted RFP-KDEL (*ER-RFP*). Note that hPro-CpepSfGFP (*green*) exhibits a dual distribution in the juxtanuclear region as well as in cell processes and subjacent to the cell membrane. Neither of these distributions matches that of ER-RFP (*red*). Both DAPI nuclear staining and a merged image are shown. *Scale bar* = 10 μm.

Gen), and experiments were performed within 6 h thereafter. Starting each experiment, cells were placed in imaging buffer (125 mM NaCl, 5.7 mM KCl, 2.5 mM $CaCl_2$, 1.2 mM $MgCl_2$, 10 mM HEPES (pH 7.4), and 0.1% BSA). Anisotropy-based FRET imaging (33) was performed on a Zeiss AxioObserver inverted microscope at 37 °C using an EC Plan-Neofluar ×40/1.30 oil lens. For fluorescence heterotransfer, excitation was 455 nm LED light filtered through a polarizer and Cyan Fluorescent Protein (CFP)-specific high-efficiency filter (Zeiss). Cyan (BP 480/40) and FRET (BP 535/30) fluorescence images were collected separately. Polarizations were split (Dual-view, Optical Insights) and detected in a single image with a Hamamatsu Orca-R2 CCD camera. Analysis was performed as described (33) using g factors calculated from the dilute fluorescein standard. For fluorescence homotransfer, experiments were performed 1 day post-transfection using 505-nm LED illumination and a high-efficiency YFP filter set for collection (Zeiss). Anisotropy images used the National Institutes of Health ImageJ software for image math and pseudocoloring. Image analysis used the Zeiss Axiovision software. Statistical tests used the Graphpad Prism software.

RESULTS

Expression of hPro-CpepSfGFP in Pancreatic β Cells—In cultured β cells and in β cells of transgenic mice expressing human proinsulin bearing emerald GFP within the connecting (C)-

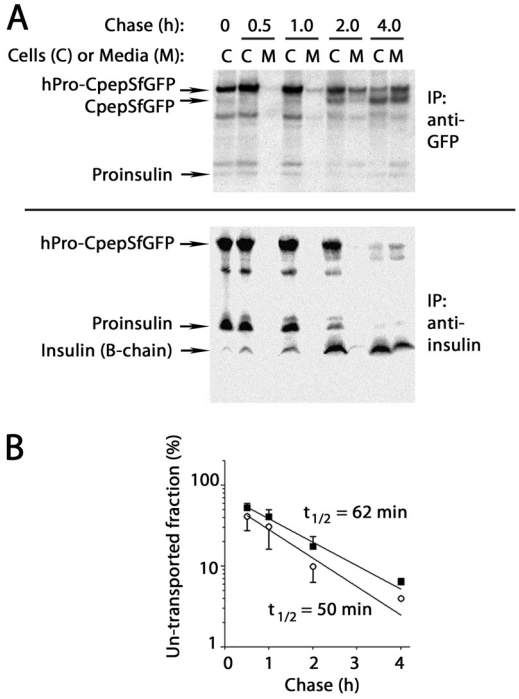

FIGURE 2. **Processing and secretion of hPro-CpepSfGFP and endogenous proinsulin in GRINCH cells.** *A*, GRINCH cells were labeled with pure ^{35}S-Cys for 0.5 h and then chased for the indicated times. At each chase time, cell lysate (*C*) and medium (*M*) were immunoprecipitated (*IP*) and resolved by reducing SDS-PAGE in 4–12% acrylamide gradient gels and analyzed by phosphorimaging. *Upper panel*, anti-GFP. *Lower panel*, anti-insulin. Note that under these conditions, the insulin A-chain is not retained on the gel. In anti-GFP immunoprecipitates, a weak band migrating midway between hPro-CpepSfGFP and CpepSfGFP is a presumptive endoproteolytic processing intermediate. This band was not consistently recovered with anti-insulin. *B*, intracellular transport rate of hPro-CpepSfGFP (■) was estimated from the data in *A* by the fraction that had been processed intracellularly to CpepSfGFP plus that secreted (regardless of processing, see text). An analogous estimate was made for the intracellular transport rate of authentic proinsulin (○). For each kind of proinsulin, the estimated untransported fraction was plotted and, assuming first-order kinetics of intracellular protein transport, a half-time of export was calculated. The data points represent the mean and range from two independent measurements.

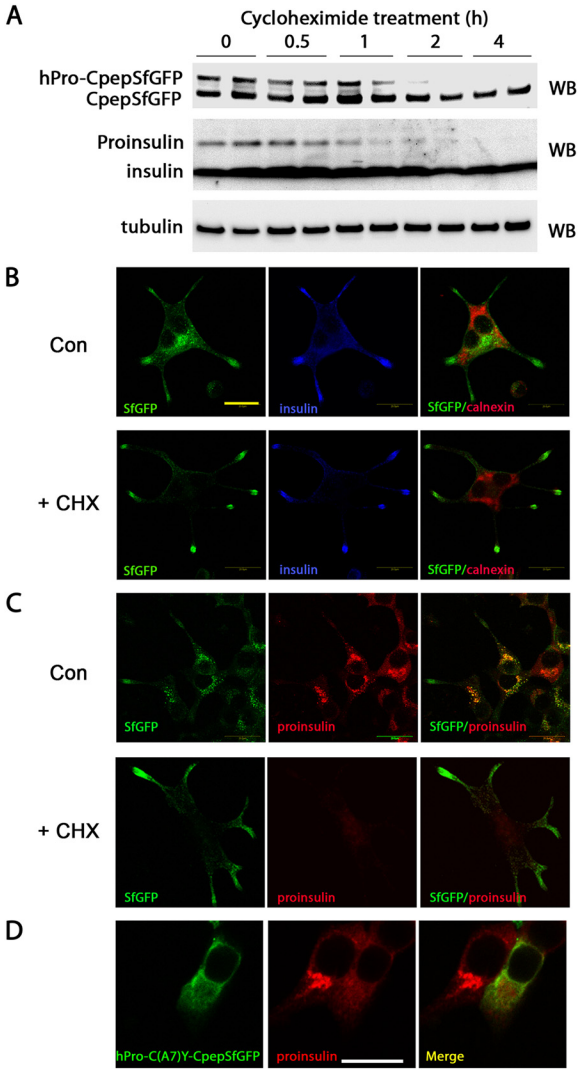

FIGURE 3. **Trafficking of hPro-CpepSfGFP in GRINCH cells.** *A*, GRINCH cells were incubated with cycloheximide (10 μg/ml, for protein synthesis inhibition) for the indicated times. At each time the cells were lysed, and the samples were resolved by reducing SDS-PAGE in 4–12% acrylamide gradient gels with electrotransfer to nitrocellulose for Western blotting (*WB*) with anti-GFP (*upper panel*), anti-insulin (*center panel*), or anti-tubulin (*lower panel*). Note the disappearance of both hPro-CpepSfGFP and proinsulin over the 4-h time course. *B–D*, images obtained by confocal microscopy. *Scale bar* = 20 μm. *B*, GRINCH cells were plated on chamber slides and were incubated 48 h later without (*Con*) or with cycloheximide (+*CHX*) for 4 h before fixation. The cells were processed for immunofluorescence with anti-insulin (*blue*) and anti-calnexin (*red*). *C*, the same cells were processed with anti-proinsulin (*red*). *D*, INS1 cells were transiently transfected with hProC(A7)Y-CpepSfGFP, fixed, and processed with anti-proinsulin. Endogenous proinsulin is clearly juxtanuclear in untransfected cells and shifts to an ER staining pattern in cells coexpressing misfolded mutant proinsulin.

peptide ("hPro-CpepGFP"), normal intracellular transport results in production of human insulin and green fluorescent C-peptide ("CpepGFP"), which are costored and cosecreted (21, 34, 35). At low cell density, INS1 (rat) β cells may extend cytoplasmic processes that accumulate secretory granules. Using such cells, anti-insulin (cross-reacting with proinsulin) detected two predominant intracellular pools of immunofluorescent protein: a juxtanuclear signal and a signal distal from the nucleus (Fig. 1*A*, *green*). In contrast, anti-proinsulin (not cross-reacting with insulin) identified one predominant pool that overlapped with juxtanuclear insulin immunofluorescence (Fig. 1*A*, *red*). In survey images, the juxtanuclear signal resembled a Golgi regional distribution, as revealed by proinsulin immunofluorescence overlapping with that of membrin (an ER-to-Golgi SNARE protein, Fig. 1*B*, *green*) or the Golgi matrix protein GM130 (*red*).

SfGFP substitutions (25) improve GFP folding/fluorescence within the oxidizing environment of the ER (26). Therefore, we expressed hPro-CpepSfGFP in INS1 cells and analyzed cells and conditioned media by immunoblotting with anti-GFP. A large fraction of hPro-CpepSfGFP was processed to CpepSfGFP, and both were recovered in conditioned medium (Fig. 1*C*). Secretion of unprocessed proinsulin and processed insulin also occurs normally from pancreatic β cells (36–38). In contrast, the *Akita*-like hProC(A7)Y-CpepSfGFP was neither processed nor secreted (Fig. 1*C*). Thus, hPro-CpepSfGFP and hProC(A7)Y-CpepSfGFP mimic the trafficking of their endogenous counterparts.

Endoproteolytic processing of hPro-CpepSfGFP should generate human insulin. To examine this, clones of stably transfected INS1 cells were screened for human insulin content and glucose-stimulated human insulin secretion. Prototypic insulin

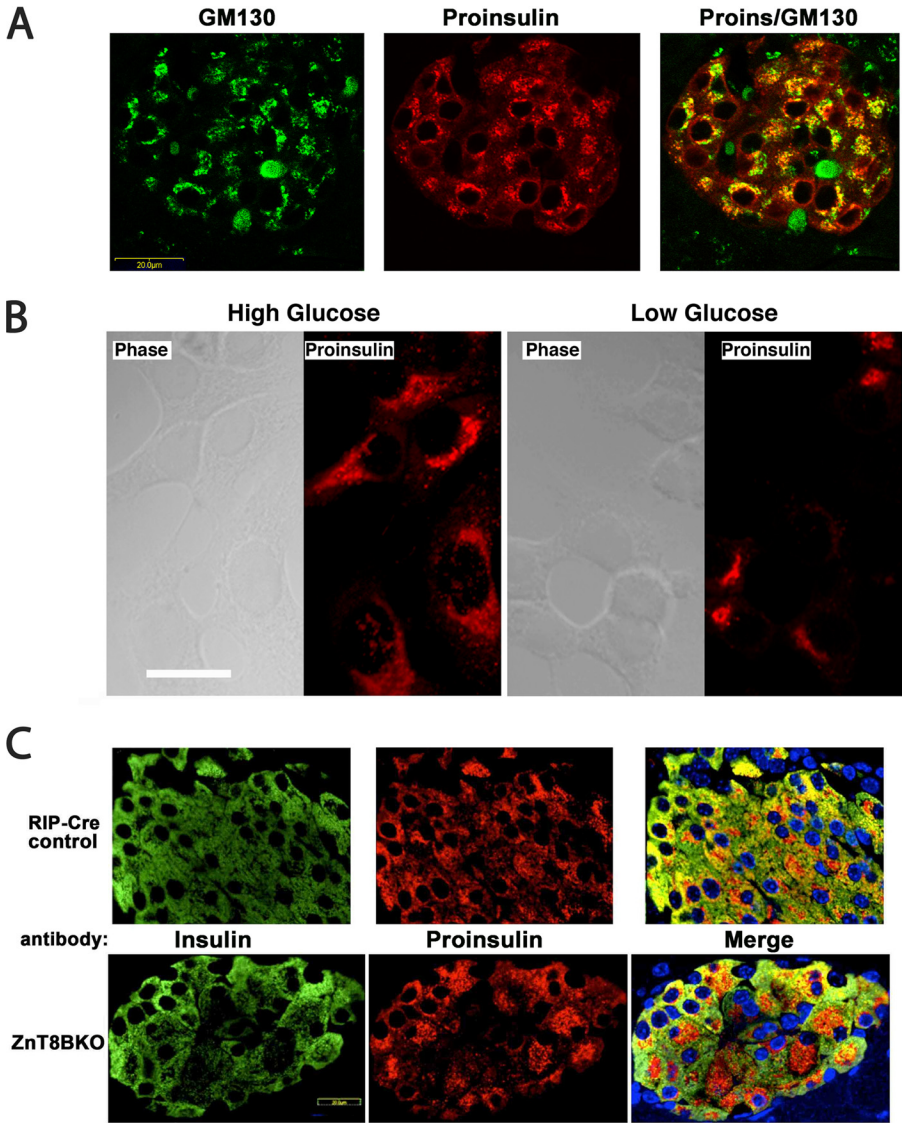

FIGURE 4. **Juxtanuclear distribution of proinsulin in islet β cells and hPro-CpepSfGFP in GRINCH cells.** *A*, pancreata from overnight fasted and 6-h refed mice were immunostained for GM130 (*green*) and proinsulin (*red*). A merged image is shown (*right panel*). Proinsulin colocalizes with the Golgi marker but also shows a blush of immunofluorescence from the ER pool. Controls proved that secondary antibody added in the second round did not cross over and react with mouse primary antibody from the first round (data not shown). *B*, GRINCH cells were cultured in high (16.7 mM) or low (2.8 mM) glucose-containing medium for 4 h, fixed, and processed for immunofluorescence with anti-proinsulin. *Scale bar* = 20 μm. *C*, paraffin blocks of *Ins2*-Cre (*RIP-Cre*) control male (*upper panels*) and litter mate ZnT8BKO (β cell-specific ZnT8 knockout mice, *lower panels*) were sectioned, deparaffinized, and processed for immunofluorescence with anti-insulin (*green*) and anti-proinsulin (*red*). Merged images, including nuclear staining (*blue*), are shown in the *right panels*. Note the expanded juxtanuclear distribution of proinsulin in the ZnT8BKO β cells.

storage and secretion was observed in several clones named GRINCH. GRINCH cells were compared with parental INS1 cells and the well established INS832/13 subclone (28). Total insulin content (rat + human) in GRINCH or INS832/13 cells was 2-fold higher than in uncloned INS1 cells (partially attributable to expression of human insulin and partially to selection of clones with favorable insulin storage). The human insulin content of GRINCH and INS832/13 cells was similar (Fig. 1*D*), and both exhibited stimulus-dependent secretion (*i.e.* net stimulated minus unstimulated) of human insulin at 12% of cellular content upon 1 h of exposure to high glucose (*E*). By SfGFP fluorescence, most GRINCH cells exhibited a hPro-CpepSfGFP-derived signal in two intracellular distributions: juxtanuclear and in cell processes or subjacent to the plasma membrane (Fig. 1*F*). This dual distribution is reminiscent of the anti-insulin immunostaining pattern (Fig. 1*A*), and neither signal overlapped significantly with that of ER-RFP (a signal peptide red fluorescent protein retrieved to the ER (31)).

GRINCH Cell Processing of hPro-CpepSfGFP—We developed evidence indicating that hPro-CpepSfGFP follows the same secretory transit pathway as that transited by proinsulin. In GRINCH cells pulse-labeled with pure ^{35}S-Cys, hPro-CpepSfGFP was processed to CpepSfGFP over a 30 min to 4 h time course (Fig. 2*A*, *upper panel*). The half-time of hPro-CpepSfGFP intracellular transport (measured by secretion and processing and mathematically corrected for removal of labeled Cys residues) was estimated at 62 min (Fig. 2*B*, ■). Anti-insulin immunoprecipitation also recovered hPro-CpepSfGFP but could simultaneously follow endogenous proinsulin. Processing to insulin also proceeded over 4 h (Fig. 2*A*, *lower panel*). The

half-time of proinsulin intracellular transport was estimated at 50 min (Fig. 2*B*, ○; note that these data were also corrected for the fact that insulin A-chains run off of these reducing gels). The small delay in transport of hPro-CpepSfGFP *versus* proinsulin can be accounted for by the larger size of the former molecule.

We also developed evidence to suggest that the Golgi distributions of hPro-CpepSfGFP and endogenous proinsulin are actively maintained by ongoing proinsulin biosynthesis. To determine whether the two pools of fluorescent protein (juxtanuclear and subplasmalemmal) corresponded to hPro-CpepSfGFP and CpepSfGFP, respectively, GRINCH cells were treated with cycloheximide (*CHX*) to block further protein synthesis. Thereafter, hPro-CpepSfGFP disappeared, shifting the ratio of immunoblotted protein strongly toward CpepSfGFP (Fig. 3*A*, *upper panel*). Over 4 h, endogenous proinsulin also disappeared (Fig. 3*A*, *center panel*). Although control cells exhibited juxtanuclear fluorescence (that did not colocalize with the ER marker calnexin, Fig. 3*B*, *upper panel*) upon inhibition of further proinsulin synthesis, GRINCH cells selectively lost their juxtanuclear fluorescence while maintaining fluorescence at the tips of processes (*lower panel*). Disappearance of juxtanuclear hPro-CpepSfGFP fluorescence (Fig. 3*C*, *left panels*) was paralleled by disappearance of immunofluorescent proinsulin (*center panels*). Disappearance of proinsulin from the Golgi region was also apparent in β cells expressing the *Akita*-like folding mutant hProC(A7)Y-CpepSfGFP (21, 34). In such cells, proinsulin immunofluorescence reverted to a pattern suggesting the ER, in which hProC(A7)Y-CpepSfGFP also accumulated (Fig. 3*D*). Thus, although proinsulin transit through the Golgi region appears rate-limiting (Fig. 3*D*, *cell at left*), its steady-state accumulation therein is dependent upon continuous delivery from the ER, and the ER step becomes a rate-limiting step in cells bearing a misfolded proinsulin expressed in *trans* (*cell at right*).

Given that steps leading to ER exit have classically been thought to be rate-limiting even in normal secretory protein trafficking (2), the predominant steady-state accumulation of proinsulin in the Golgi region (rather than in the ER) seemed surprising. Yet, when proinsulin biosynthesis is up-regulated at the ER, one would expect that its detection at the ER should increase. To test this, we modified a rodent fasting/refeeding protocol to try to synchronize feeding (39). In the islets of mice fasted overnight without refeeding, proinsulin was found essentially exclusively in the Golgi region (not shown), whereas in mice then refed for 6 h, a "blush" of proinsulin immunofluorescence was detected in an ER pattern (Fig. 4*A*, *red*) beyond the proinsulin concentrated in the Golgi region (*GM130*, *green*). Similarly, we examined GRINCH cells incubated in high (16.7 mM) or low (2.8 mM) glucose for 4 h. In high glucose, proinsulin showed a distribution that included the juxtanuclear Golgi region but also extended beyond it toward the cell periphery. In low glucose, proinsulin tended to concentrate more exclusively in the juxtanuclear Golgi region (Fig. 4*B*). Further, in mice with β cell-specific knockout of ZnT8 that transports zinc needed for proinsulin hexamerization, even in randomly fed animals (Fig. 4*C*), when averaged over 840 insulin-positive cells, the Golgi proinsulin area appeared 2.4-fold greater than in rat insulin promoter (RIP)-Cre control mice (quantified as described under "Experimental Procedures"). Thus, ER and Golgi proinsulin distributions appear to be influenced by physiological conditions that affect proinsulin synthesis rate and proinsulin hexamerization.

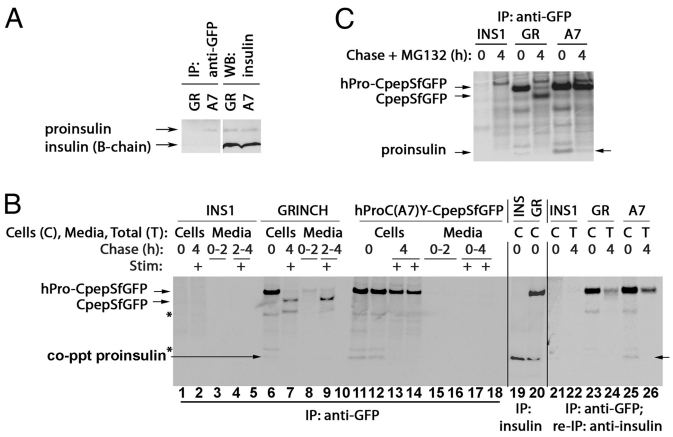

FIGURE 5. **Wild-type and mutant hPro-CpepSfGFP coprecipitate endogenous proinsulin.** *A*, GRINCH (*GR*) and hProC(A7)Y-CpepSfGFP (*A7*) cells were either lysed and resolved by reducing SDS-PAGE in 4–12% acrylamide gradient gels and electrotransfer to nitrocellulose for direct immunoblotting (*WB*) with anti-insulin (*second set of lanes*) or immunoprecipitated (*IP*) with anti-GFP antibodies before proceeding with the same immunoblotting analysis (*first set of lanes*). Note that hProC(A7)Y-CpepSfGFP cells do not have increased intracellular proinsulin, yet anti-GFP immunoprecipitation selectively coprecipitates endogenous proinsulin from hProC(A7)Y-CpepSfGFP cells. *B*, parental INS1 (*INS*), GRINCH, and hProC(A7)Y-CpepSfGFP cells were labeled with ^{35}S-Met/Cys for 30 min, chased for the first 2 h under unstimulated (low glucose) conditions, and then stimulated with secretagogue (*Stim:* +) for another 2 h. The media were collected, and the cells were lysed at the indicated chase times. The samples were immunoprecipitated with anti-GFP antibodies (*lanes 1–18*, *lanes 5* and 10 are blanks), resolved using reducing SDS-PAGE in 4–12% acrylamide gradient gels, and analyzed by phosphorimaging. As a control for the positions of hPro-CpepSfGFP and proinsulin bands, INS1 and GRINCH cells were labeled with ^{35}S-Met/Cys for 1 h and immunoprecipitated with anti-insulin (*lanes 19* and *20*). Note that after stimulation, processed CpepSfGFP was robustly secreted from GRINCH cells (*lane 9*). In *lanes 21-26*, cells were labeled and chased, and samples were collected as before, but the 4-h media and cell lysates were combined into a single sample to generate total (*T*). Anti-GFP immunoprecipitates samples were then reboiled in SDS, diluted into complete immunoprecipitation buffer, reimmunoprecipitated with anti-insulin, resolved using SDS-PAGE in 4–12% acrylamide gradient gels, and analyzed by phosphorimaging. Note that coprecipitation (*co-ppt*) of endogenous proinsulin became undetectable after a 4-h chase (*lanes 7, 13, 14,* and *26*). The identities of the two bands marked with *asterisks* are unknown. *C*, parental INS1, GRINCH, and hProC(A7)Y-CpepSfGFP cells were labeled with ^{35}S-Met/Cys as in *B* but either lysed immediately or chased for 4 h in the presence of 10 μM MG132 before immunoprecipitation with anti-GFP and analysis as in *B*. Loss of proinsulin coprecipitation with hProC(A7)Y-SfCpepGFP was at least in part related to ERAD because some endogenous proinsulin could still be coprecipitated at 4 h in cells treated with MG132 (*arrow at right*). In contrast, loss of the weak endogenous proinsulin coprecipitation with hPro-CpepSfGFP in GRINCH cells corresponds to processing to insulin and CpepSfGFP, consistent with Fig. 2*A*.

Normal and Abnormal Proinsulin Assembly—We noted that endogenous proinsulin was weakly coprecipitated with hPro-CpepSfGFP (Fig. 2*A*). To examine the extent of WT-WT *versus* WT-mutant subunit association, we prepared INS1 cells stably expressing the *Akita*-like folding mutant hProC(A7)Y-SfCpepGFP ("A7"). When comparing cells containing the same overall level of endogenous proinsulin, mutant hProC(A7)Y-CpepGFP coprecipitated more total proinsulin than wild-type hPro-CpepSfGFP in GRINCH cells (Fig. 5*A*). Also, hProC(A7)Y-SfCpepGFP coprecipitated more newly synthesized endogenous proinsulin bands (Fig. 5*B*, *lanes 11* and *12*, match the band

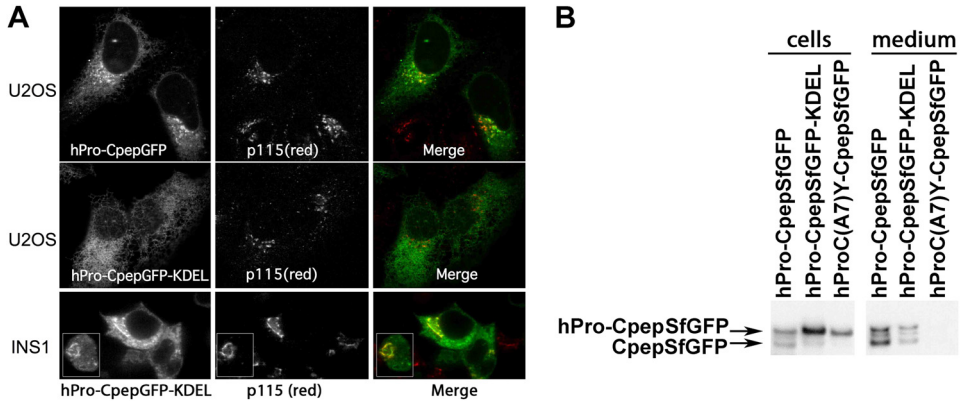

FIGURE 6. **Expression of hPro-CpepSfGFP bearing a carboxyl-terminal KDEL sequence.** *A*, U2OS cells were transiently transfected with hPro-CpepSfGFP either not bearing (*upper panels*) or bearing a KDEL retrieval sequence (*center panels*). INS1 cells were similarly transfected with hPro-CpepGFP bearing a carboxyl-terminal KDEL (*lower panels*), and each transfection was processed for indirect immunofluorescence of the Golgi marker p115 (Ref. 55, antibody from Dr. D. Shields, Albert Einstein College of Medicine) as well as direct green fluorescence. The *inset* shows that in INS1 cells with a smaller rounder morphology, the Golgi appears as a unique circular-shaped structure that is decorated with the KDEL-tagged green fluorescent proinsulin. Merged images are shown in the *right panels*. *Scale bar* = 10 μm. *B*, INS1 cells were transiently transfected with hPro-CpepSfGFP, hPro-CpepSfGFP bearing a carboxyl-terminal KDEL retrieval signal, or hProC(A7)Y-CpepSfGFP. Samples were processed exactly as in Fig. 1*C*.

mobility of proinsulin immunoprecipitated from control cells in *lanes 19* and *20*). Indeed, when hProC(A7)Y-SfCpepGFP immunoprecipitates were reimmunoprecipitated with anti-insulin, recovery of endogenous proinsulin was confirmed (Fig. 5*B*, *lane 25*), and when proteasome inhibitor MG132 was included during the chase, coprecipitation of endogenous proinsulin was still detectable even 4 h after synthesis (*C*). Together, the data indicate that WT-WT proinsulin association results in less coprecipitation but is consistent with rapid ER export to the Golgi region, whereas WT-mutant proinsulin association increases coprecipitation between the partners and results shifts the rate-limiting step of wild-type intracellular transport to the ER.

Cross-dimerization of proinsulin may generate interesting outcomes. We expressed a novel hPro-CpepGFP-KDEL construct in U2OS osteosarcoma cells that lack endogenous proinsulin and in INS1 cells. In U2OS cells, unlike the secretory form of hPro-CpepGFP (Fig. 6*A*, *upper panels*), hPro-CpepGFP-KDEL was not detectably secreted and was observed in an ER-like intracellular distribution that hardly overlapped with the juxtanuclear Golgi region (*center panels*). In contrast, in INS1 cells, hPro-CpepGFP-KDEL exhibited a distribution that was both ER-like and also overlapped with the Golgi region (Fig. 6*A*, *bottom panels*). Moreover, in INS1 cells, hPro-CpepSfGFP-KDEL was both processed (to CpepSfGFP) and secreted (Fig. 6*B*), including human insulin secretion ranging from 12–20% of that obtained from control INS1 cells expressing hPro-CpepSfGFP (data not shown). Thus, ER-retained hPro-CpepGFP-KDEL can be "hijacked" and exported from cells in which association with endogenous proinsulin is possible.

Proinsulin Associations Measured by FRET—There are no reported studies of oligomeric assembly of any secretory protein in living mammalian cells (although some membrane proteins have been examined). We employed hPro-CpepSfCerulean (blue fluorescent protein) and hPro-CpepSfVenus (YFP) to perform *in situ* FRET. Similar to hPro-CpepSfGFP, when transiently expressed in INS1 cells, hPro-CpepSfCerulean and hPro-CpepSfVenus were each processed to the appropriate Cpep fluorescent product that exhibited stimulated exocytosis (Fig. 7*A*, *left panel*). Overnight human insulin secretion from INS1 cells transiently transfected with hPro-CpepSfGFP, hPro-CpepSfCerulean, or hPro-CpepSfVenus was comparable (Fig. 7*B*). Moreover, hPro-CpepSfCerulean and hPro-CpepSfVenus exhibited significant entry into INS1 cell processes (Fig. 7*C*), indicating that these chimeric proteins are also suitable surrogates for studies of proinsulin trafficking. Similar to the hProC(A7)Y-CpepSfGFP mutant, both the hProC(A7)Y-CpepSfCerulean and hProC(A7)Y-CpepSfVenus mutants were blocked in processing or secretion (Fig. 7*A*, *right panel*).

We next attempted anisotropy-based FRET (40) to look at interactions of WT-WT or WT-mutant proinsulin expressed recombinantly in live COS7 cells. Cells were cotransfected with a pair of SfCerulean- and SfVenus-labeled constructs, including an ER-localized SfCerulean-KDEL (Fig. 8*A*). Anisotropies of SfCerulean fluorescence were high in all cases (Fig. 8*A*, *third row, blue pseudocolor*). Depolarized FRET fluorescence (SfCerulean excitation, SfVenus collection), indicating protein-protein interaction, was detected in cells expressing both WT-WT and WT-mutant proinsulin pairs (Fig. 8*A*, *bottom panel, orange pseudocolor*). Conversely, in the "FRET channel," anisotropy (absence of detectable protein-protein interaction) remained high when either hPro-CpepSfVenus or hProC(A7)Y-CpepSfVenus was coexpressed with an ER-localized SfCerulean-containing control protein (Fig. 8*A*, *bottom panel, blue pseudocolor*). The data indicate specific WT-WT and WT-mutant proinsulin interactions in the secretory pathway of live COS7 cells.

We then repeated these experiments in transiently transfected INS1 β cells (Fig. 8, *B* and *C*). Specific interaction patterns were identical to those obtained in COS7 cells. However, the measured amount of FRET was diminished in INS1 cells (Fig. 8*C*, note *y-axes*), consistent with competitive binding by endogenous proinsulin molecules to their respective fluorescent partners.

To further explore differences in affinity of cross-dimerization suggested by our immunoprecipitation experiments (Fig.

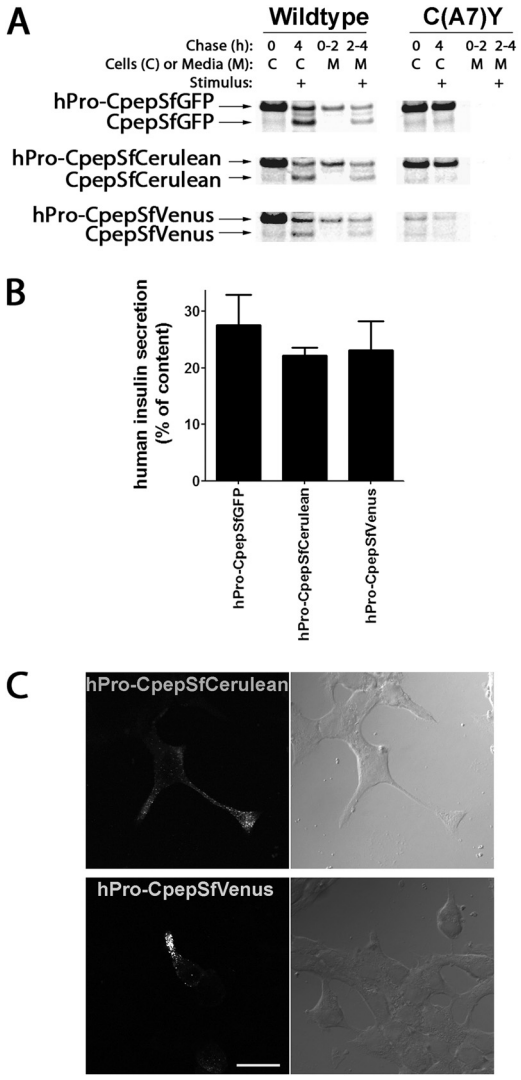

FIGURE 7. **Expression of hPro-CpepSfGFP, hPro-CpepSfCerulean or hPro-CpepSfVenus in INS1 cells.** *A*, INS1 cells transiently transfected with wild-type hPro-CpepSfGFP (*upper panels*), hPro-CpepSfCerulean (*center panels*), or hPro-CpepSfVenus (*lower panels*) not bearing (*left panels*) or bearing the C(A7)Y point mutation (*right panels*) were labeled with ^{35}S-Met/Cys for 30 min, chased for 2 h under unstimulated (low glucose) conditions, and then chased for another 2 h in the presence of stimulus before final cell lysis. Each sample was immunoprecipitated with anti-GFP, resolved by reducing SDS-PAGE on 4–12% acrylamide gradient gels, and analyzed by phosphorimaging. *B*, INS1 cells transiently transfected with hPro-CpepSfGFP, hPro-CpepSfCerulean, or hPro-CpepSfVenus were plated in 12-well plates. At 20 h post-transfection, the bathing medium was replaced and collected for a further 18 h, and the cells were lysed. The fractional secretion of human insulin was measured by specific RIA. Data represent the mean ± S.D. from three independent experiments. *C*, INS1 cells transiently transfected to express hPro-CpepSfCerulean or hPro-CpepSfVenus as in *A* were treated with cycloheximide as in Fig. 3*B*. Phase micrographs (*right panels*) contain fields of cells including those expressing direct blue (*upper panels*) or yellow fluorescent (*lower panels*) proteins. Both products accumulated in cell processes, indicating secretory granule accumulation. *Scale bar* = 20 μm.

5), we also studied COS7 cells expressing single hPro-CpepSfVenus or hProC(A7)Y-CpepSfVenus fusion proteins to examine homotransfer FRET by fluorescence polarization microscopy (Fig. 8*D*). Homotransfer (loss of anisotropy) between two yellow fluorescent proteins is less efficient than cyan:yellow FRET (41). Homotransfer was only observed (42) upon overexpression in COS7 cells (Fig. 8*D*). Homotransfer FRET was observed for hProC(A7)Y-CpepSfVenus at lower relative fluorescence than for hPro-CpepSfVenus, suggesting that mutant proinsulin has a higher affinity for association than wild-type proinsulin.

DISCUSSION

Assembly/oligomerization is linked to the kinetics of secretory protein trafficking, with ER exit thought to be rate-limiting (10–13). In pancreatic β cells, signal peptide cleavage initiates proinsulin monomer folding (43). Sometime thereafter, proinsulin dimerizes (44) and then, facilitated by zinc, progresses to hexamers (15, 19). After endoproteolytic processing in secretory granules, multimerization of processed insulin proceeds (14, 45). However, the timing of proinsulin assembly relative to its transport has been difficult to study.

In this study, we developed the GRINCH β cell line (which exhibits excellent glucose-stimulated insulin secretion) to examine intracellular hPro-CpepSfGFP and CpepSfGFP fluorescent distributions. In these cells, we "rediscovered" an established fact: at steady-state, the dominant intracellular pool of both endogenous and fluorescent proinsulin appears in the juxtanuclear Golgi region rather than the ER (Fig. 1). This is also true in β cells of normal rat islets (1, 46), mouse islets (4, 47), and human islets (48, 49). On the one hand, the steady-state localization of proinsulin approximates that of Golgi matrix proteins and the ER-to-Golgi SNARE protein membrin (Fig. 1*B*). This localization (50) would seemingly position proinsulin accumulation on the *cis* side of the Golgi complex. On the other hand, by immunoelectron microscopy, steady-state proinsulin accumulation is found largely within stacked Golgi cisternae (1, 51) and in forming secretory granules on the *trans* face of the Golgi complex (52).

In GRINCH cells, hPro-CpepSfGFP trafficking recapitulates proinsulin trafficking, including Golgi accumulation, despite the fact that the folding time of hPro-CpepSfGFP is lengthened sufficiently (compared with endogenous proinsulin, which is ~4 times smaller than hPro-CpepSfGFP) to delay its transit to processed/secreted products (Fig. 2). Nevertheless, the Golgi localization of proinsulin and hPro-CpepSfGFP is fed continuously by a stream of proinsulin molecules running directly from ER biosynthesis (Fig. 3). For Golgi export to be the slowest step in proinsulin and hPro-CpepSfGFP trafficking implies one or more as-yet-unidentified molecular events therein. Indeed, only under conditions in which proinsulin synthesis is up-regulated does an appreciable ER concentration of proinsulin become evident (Fig. 4, *A* and *B*). We do not yet know how hexameric assembly fits into Golgi trafficking of proinsulin, but because subunit association of secretory proteins is thought to be rate-limiting in intracellular transport (10–13), we are struck by the observation that deficiency of zinc (which ordinarily is incorporated into proinsulin hexamers in islet β cells) expands proinsulin accumulation in the Golgi region (Fig. 4*C*), although loss of ZnT8 does not block processing to mature insulin (53). We caution that animals with β cell-specific ZnT8 deletion are glucose-intolerant and thereby predisposed to synthesize more proinsulin (32). Thus, more work is needed to demonstrate conclusively how dimeric followed by hexameric assembly of proinsulin contributes to the regulation of proinsulin trafficking.

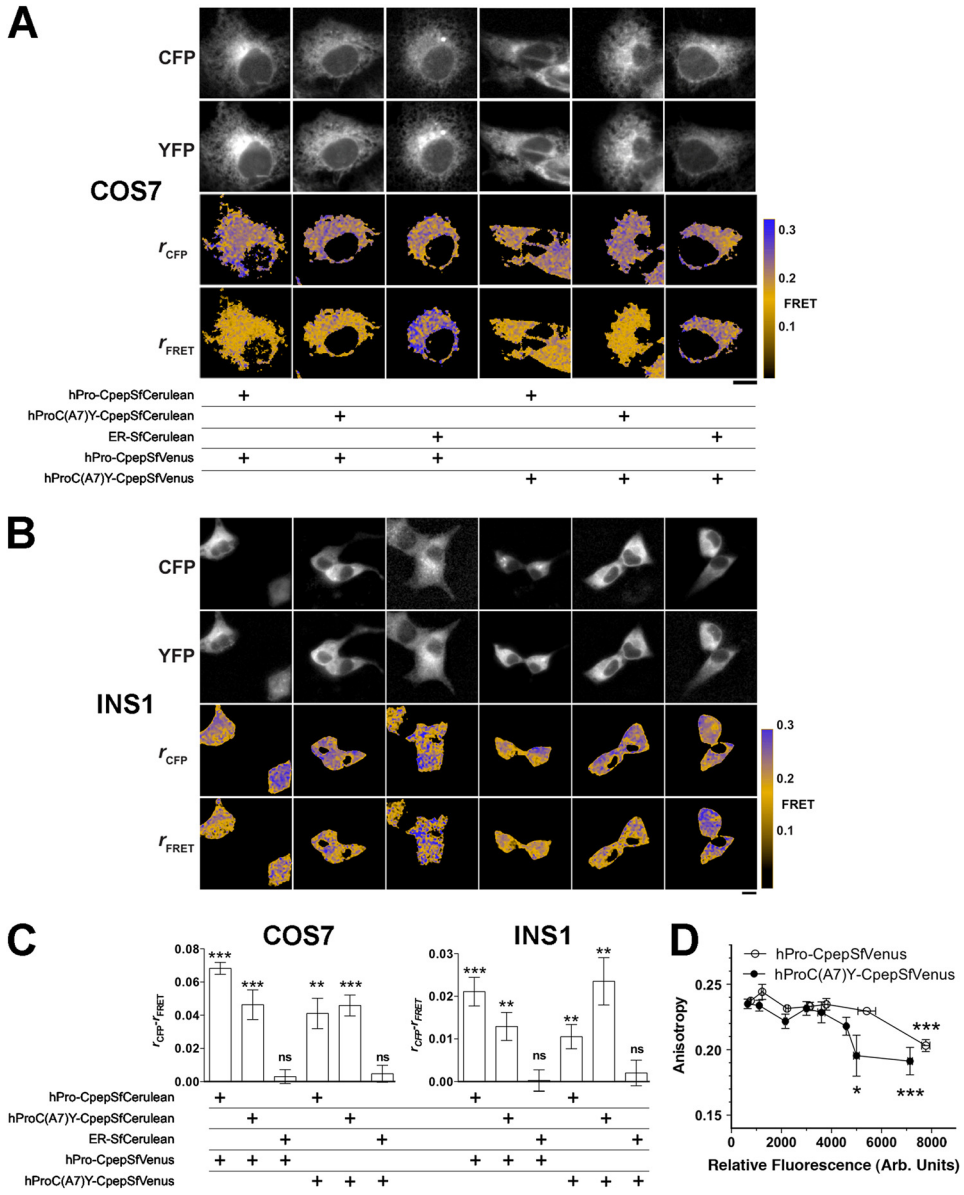

FIGURE 8. **Interactions of hPro-Cpep and hProC(A7)Y-Cpep in living cells as determined by FRET.** *A* and *B*, hPro-Cpep and hProC(A7)Y-Cpep fusions with SfCerulean and SfVenus were cotransfected into COS7 (*A*) and INS1 cells (*B*) in the indicated combinations along with ER-localized control protein. Cells were observed by fluorescence polarization microscopy 6 h post-transfection for COS7 cells and 24 h post-transfection for Ins1 cells. The *top two rows* of images display cyan (*CFP*) and yellow fluorescence (*YFP*), and the *bottom two rows* display the calculated anisotropies (*r*) for the CFP and FRET images (cyan excitation, yellow emission). Reduction in the FRET channel anisotropy (*orange*) relative to the cyan anisotropy indicates FRET. Non-cellular regions in the anisotropy images were masked for clarity (*black*). *Scale bar* = 10 μm. *C*, the difference between fluorescence anisotropies in CFP and FRET channels was calculated from image data obtained in COS7 and INS1 cells. Significant FRET was observed between homotypic and heterotypic expression of proinsulin constructs in both cell types but not when either construct was coexpressed with an ER-localized control plasmid. $n = 10$ cells per group; *, $p < 0.05$, **, $p < 0.01$; ***, $p < 0.001$, Student's *t* test *versus* 0. *D*, to look at the relative strength of protein-protein interactions between hPro-CpepSfVenus or hProC(A7)Y-CpepSfVenus homotypic pairs, fusion protein overexpression was achieved in COS7 cells by waiting 17 h post-transfection. Homotransfer FRET is indicated by a reduction in SfVenus anisotropy and was observed with less relative fluorescence (expressed in arbitrary units) for hProC(A7)Y-CpepSfVenus compared with hPro-Cpep-SfVenus, consistent with an increased affinity (analysis of variance, Tukey multiple comparison test *versus* lowest detectable expression, $n \geq 3$ cells for each point. *, $p < 0.05$; ***, $p < 0.001$). *Bars* indicate mean ± S.E. for *B* and *C*.

It is now certain that proinsulin has already dimerized by the time it enters the Golgi region. First, hPro-CpepSfGFP coprecipitates endogenous proinsulin through noncovalent interactions, even at the zero chase time. Second, human proinsulin KDEL that is nonsecreted and resides almost exclusively in the ER of non-β cells, is "forward-shifted" in INS1 cells synthesizing endogenous rat proinsulin (Fig. 6*A*), even to the point of being converted to human insulin/CpepSfGFP and becoming secreted (Fig. 6*B*). Importantly, a KDEL-containing ER-RFP is not forwarded-shifted in such cells (Fig. 1*F*). Most importantly, using anisotropy-based FRET, we have made the first direct demonstration of recombinant WT-WT proinsulin interaction that can be seen within the ER (Fig. 8*A*). The FRET signal in this instance is not merely due to the proteins being contained in the ER. Indeed, FRET is not observed in the pairing of hPro-CpepSfVenus with an ER-retained SfCerulean (Fig. 8, *A*–*C*). Rather, FRET represents a specific intermolecular interaction between proinsulin molecules that is actually decreased in INS1

cells bearing endogenous proinsulin, which serves as a competing dimerization partner, consistent with our observation of coprecipitation between recombinant and endogenous proinsulin (Figs. 2 and 5).

The situation changes fairly drastically when one of the proinsulin partners is a mutant proinsulin responsible for the syndrome of mutant Ins-gene induced diabetes of youth (9). We have previously proposed the alternatives (that are not mutually exclusive) that in heterozygous individuals, proinsulin mutants causing mutant Ins-gene induced diabetes of youth might directly engage wild-type proinsulin in protein complexes or might indirectly recruit wild-type proinsulin into such complexes via changes in the oxidizing environment of the ER (9). In this study, cross-dimerization is linked to blockade of coexpressed hPro-CpepSfGFP, shifting its steady-state distribution from the Golgi region to the ER (Fig. 3*D*). Retention of coexpressed wild-type proinsulin does not appear to be merely secondary to ER stress (54). Rather, blockade *in trans* is immediately associated with increased coprecipitation of wild-type proinsulin (Fig. 5) and a more easily detectable cross-dimerization FRET signal (Fig. 8, *B* and *C*). Again, misfolding and retention of mutant proinsulin in the ER still does not generate a FRET signal with an unrelated ER-retained SfCerulean, indicating that mere retention in the ER is not sufficient to produce nonspecific protein interaction.

In conclusion, we report that the steady-state accumulation of wild-type proinsulin is maintained dynamically (and physiologically) with surprising accumulation in the Golgi region. However, *in trans*, wild-type proinsulin can cross-dimerize with misfolded proinsulin in β cells, and with this, the rate-limiting step in intracellular transport of wild-type proinsulin is shifted to the ER. These data may provide helpful clues in the analysis of β cell dysfunction during progression of type 2 diabetes.

Acknowledgments—We thank ALPCO for supplying the proinsulin-specific antibody used for immunocytochemistry, Ms. Lindsey Costantini for creation of the SfVenus and SfCerulean cDNAs, and Mr. Paul Gianella for creating hPro-CpepSfGFP-KDEL. We also thank the laboratory of Dr. C. Newgard (Duke University, Durham NC) for supplying INS832/13 cells, the Morphology and Image Analysis Core and the Molecular Biology and DNA Sequencing Core of the National Institutes of Health-funded Diabetes Research Center (NIH P60-DK20572) for assistance, and Bill and Dee Brehm for helping to create the Brehm Center for Diabetes Research at the University of Michigan and their support of the Brehm Coalition.

REFERENCES

1. Orci, L., Ravazzola, M., Amherdt, M., Madsen, O., and Vassalli, J. D. (1985) Direct identification of prohormone conversion site in insulin-secreting cells. *Cell* **42,** 671–681
2. Lodish, H. F. (1988) Transport of secretory and membrane glycoproteins from the rough endoplasmic reticulum to the Golgi. A rate-limiting step in protein maturation and secretion. *J. Biol. Chem.* **263,** 2107–2110
3. Scheuner, D., Vander Mierde, D., Song, B., Flamez, D., Creemers, J. W., Tsukamoto, K., Ribick, M., Schuit, F. C., and Kaufman, R. J. (2005) Control of mRNA translation preserves endoplasmic reticulum function in β cells and maintains glucose homeostasis. *Nat. Med.* **11,** 757–764
4. Gupta, S., McGrath, B., and Cavener, D. R. (2010) PERK (EIF2AK3) regulates proinsulin trafficking and quality control in the secretory pathway. *Diabetes* **59,** 1937–1947
5. Zito, E., Chin, K. T., Blais, J., Harding, H. P., and Ron, D. (2010) ERO1-β, a pancreas-specific disulfide oxidase, promotes insulin biogenesis and glucose homeostasis. *J. Cell Biol.* **188,** 821–832
6. Khoo, C., Yang, J., Rajpal, G., Wang, Y., Liu, J., Arvan, P., and Stoffers, D. A. (2011) Endoplasmic reticulum oxidoreductin-1-like β (ERO1lβ) regulates susceptibility to endoplasmic reticulum stress and is induced by insulin flux in β-cells. *Endocrinology* **152,** 2599–2608
7. Castle, A. M., Stahl, L. E., and Castle, J. D. (1992) A 13-amino acid N-terminal domain of a basic proline-rich protein is necessary for storage in secretory granules and facilitates exit from the endoplasmic reticulum. *J. Biol. Chem.* **267,** 13093–13100
8. Rajpal, G., Schuiki, I., Liu, M., Volchuk, A., and Arvan, P. (2012) Action of protein disulfide isomerase on proinsulin exit from endoplasmic reticulum of pancreatic β-cells. *J. Biol. Chem.* **287,** 43–47
9. Liu, M., Hodish, I., Haataja, L., Lara-Lemus, R., Rajpal, G., Wright, J., and Arvan, P. (2010) Proinsulin misfolding and diabetes. Mutant INS gene-induced diabetes of youth. *Trends Endocrinol. Metab.* **21,** 652–659
10. Rose, J. K., and Doms, R. W. (1988) Regulation of protein export from the endoplasmic reticulum. *Annu. Rev. Cell Biol.* **4,** 257–288
11. Pelham, H. R. (1989) Control of protein exit from the endoplasmic reticulum. *Annu. Rev. Cell Biol.* **5,** 1–23
12. Hurtley, S. M., and Helenius, A. (1989) Protein oligomerization in the endoplasmic reticulum. *Ann. Rev. Cell Biol.* **5,** 277–307
13. Gething, M. J., and Sambrook, J. (1990) Transport and assembly processes in the endoplasmic reticulum. *Semin. Cell Biol.* **1,** 65–72
14. Michael, J., Carroll, R., Swift, H. H., and Steiner, D. F. (1987) Studies on the molecular organization of rat insulin secretory granules. *J. Biol. Chem.* **262,** 16531–16535
15. Dodson, G., and Steiner, D. (1998) The role of assembly in insulin's biosynthesis. *Curr. Opin. Struct. Biol.* **8,** 189–194
16. Frank, B. H., and Veros, A. J. (1970) Interaction of zinc with proinsulin. *BBRC* **38,** 284–289
17. Chimienti, F., Devergnas, S., Favier, A., and Seve, M. (2004) Identification and cloning of a beta-cell-specific zinc transporter, ZnT-8, localized into insulin secretory granules. *Diabetes* **53,** 2330–2337
18. Chimienti, F., Devergnas, S., Pattou, F., Schuit, F., Garcia-Cuenca, R., Vandewalle, B., Kerr-Conte, J., Van Lommel, L., Grunwald, D., Favier, A., and Seve, M. (2006) *In vivo* expression and functional characterization of the zinc transporter ZnT8 in glucose-induced insulin secretion. *J. Cell Sci.* **119,** 4199–4206
19. Huang, X. F., and Arvan, P. (1995) Intracellular transport of proinsulin in pancreatic β cells. Structural maturation probed by disulfide accessibility. *J. Biol. Chem.* **270,** 20417–20423
20. Watkins, S., Geng, X., Li, L., Papworth, G., Robbins, P. D., and Drain, P. (2002) Imaging secretory vesicles by fluorescent protein insertion in propeptide rather than mature secreted peptide. *Traffic* **3,** 461–471
21. Liu, M., Hodish, I., Rhodes, C. J., and Arvan, P. (2007) Proinsulin maturation, misfolding, and proteotoxicity. *Proc. Natl. Acad. Sci. U.S.A.* **104,** 15841–15846
22. Meur, G., Simon, A., Harun, N., Virally, M., Dechaume, A., Bonnefond, A., Fetita, S., Tarasov, A. I., Guillausseau, P. J., Boesgaard, T. W., Pedersen, O., Hansen, T., Polak, M., Gautier, J. F., Froguel, P., Rutter, G. A., and Vaxillaire, M. (2010) Insulin gene mutations resulting in early-onset diabetes: marked differences in clinical presentation, metabolic status, and pathogenic effect through endoplasmic reticulum retention. *Diabetes* **59,** 653–661
23. Rajan, S., Eames, S. C., Park, S. Y., Labno, C., Bell, G. I., Prince, V. E., and Philipson, L. H. (2010) *In vitro* processing and secretion of mutant insulin proteins that cause permanent neonatal diabetes. *Am. J. Physiol. Endocrinol. Metab.* **298,** E403–410
24. Jain, R. K., Joyce, P. B., Molinete, M., Halban, P. A., and Gorr, S. U. (2001) Oligomerization of green fluorescent protein in the secretory pathway of endocrine cells. *Biochem. J.* **360,** 645–649
25. Pédelacq, J. D., Cabantous, S., Tran, T., Terwilliger, T. C., and Waldo, G. S. (2006) Engineering and characterization of a superfolder green fluorescent protein. *Nat. Biotechnol.* **24,** 79–88

26. Aronson, D. E., Costantini, L. M., and Snapp, E. L. (2011) Superfolder GFP is fluorescent in oxidizing environments when targeted via the Sec translocon. *Traffic* **12,** 543–548
27. Asfari, M., Janjic, D., Meda, P., Li, G., Halban, P. A., and Wollheim, C. B. (1992) Establishment of 2-mercaptoethanol-dependent differentiated insulin-secreting cell lines. *Endocrinology* **130,** 167–178
28. Hohmeier, H. E., Mulder, H., Chen, G., Henkel-Rieger, R., Prentki, M., and Newgard, C. B. (2000) Isolation of INS-1-derived cell lines with robust ATP-sensitive K+ channel-dependent and -independent glucose-stimulated insulin secretion. *Diabetes* **49,** 424–430
29. Rizzo, M. A., Springer, G. H., Granada, B., and Piston, D. W. (2004) An improved cyan fluorescent protein variant useful for FRET. *Nat. Biotechnol.* **22,** 445–449
30. Nagai, T., Ibata, K., Park, E. S., Kubota, M., Mikoshiba, K., and Miyawaki, A. (2002) A variant of yellow fluorescent protein with fast and efficient maturation for cell-biological applications. *Nat. Biotechnol.* **20,** 87–90
31. Snapp, E. L., Sharma, A., Lippincott-Schwartz, J., and Hegde, R. S. (2006) Monitoring chaperone engagement of substrates in the endoplasmic reticulum of live cells. *Proc. Natl. Acad. Sci. U.S.A.* **103,** 6536–6541
32. Wijesekara, N., Dai, F. F., Hardy, A. B., Giglou, P. R., Bhattacharjee, A., Koshkin, V., Chimienti, F., Gaisano, H. Y., Rutter, G. A., and Wheeler, M. B. (2010) β Cell-specific Znt8 deletion in mice causes marked defects in insulin processing, crystallisation and secretion. *Diabetologia* **53,** 1656–1668
33. Piston, D. W., and Rizzo, M. A. (2008) FRET by fluorescence polarization microscopy. *Methods Cell Biol.* **85,** 415–430
34. Hodish, I., Absood, A., Liu, L., Liu, M., Haataja, L., Larkin, D., Al-Khafaji, A., Zaki, A., and Arvan, P. (2011) *In vivo* misfolding of proinsulin below the threshold of frank diabetes. *Diabetes* **60,** 2092–2101
35. Hodish, I., Liu, M., Rajpal, G., Larkin, D., Holz, R. W., Adams, A., Liu, L., and Arvan, P. (2010) Misfolded proinsulin affects bystander proinsulin in neonatal diabetes. *J. Biol. Chem.* **285,** 685–694
36. Kuliawat, R., and Arvan, P. (1992) Protein targeting via the "constitutive-like" secretory pathway in isolated pancreatic islets. Passive sorting in the immature granule compartment. *J. Cell Biol.* **118,** 521–529
37. Kuliawat, R., Klumperman, J., Ludwig, T., and Arvan, P. (1997) Differential sorting of lysosomal enzymes out of the regulated secretory pathway in pancreatic β-cells. *J. Cell Biol.* **137,** 595–608
38. Lara-Lemus, R., Liu, M., Turner, M. D., Scherer, P., Stenbeck, G., Iyengar, P., and Arvan, P. (2006) Lumenal protein sorting to the constitutive secretory pathway of a regulated secretory cell. *J. Cell Sci.* **119,** 1833–1842
39. Giddings, S. J., Chirgwin, J., and Permutt, M. A. (1981) The effects of fasting and feeding on preproinsulin messenger RNA in rats. *J. Clin. Invest.* **67,** 952–960
40. Rizzo, M. A., and Piston, D. W. (2005) High-contrast imaging of fluorescent protein FRET by fluorescence polarization microscopy. *Biophys. J.* **88,** L14–16
41. Rizzo, M. A., Springer, G., Segawa, K., Zipfel, W. R., and Piston, D. W. (2006) Optimization of pairings and detection conditions for measurement of FRET between cyan and yellow fluorescent proteins. *Microsc. Microanal.* **12,** 238–254
42. Lidke, D. S., Nagy, P., Barisas, B. G., Heintzmann, R., Post, J. N., Lidke, K. A., Clayton, A. H., Arndt-Jovin, D. J., and Jovin, T. M. (2003) Imaging molecular interactions in cells by dynamic and static fluorescence anisotropy (rFLIM and emFRET). *Biochem. Soc. Trans.* **31,** 1020–1027
43. Liu, M., Lara-Lemus, R., Shan, S. O., Wright, J., Haataja, L., Barbetti, F., Guo, H., Larkin, D., and Arvan, P. (2012) Impaired cleavage of preproinsulin signal peptide linked to autosomal-dominant diabetes. *Diabetes* **61,** 828–837
44. Frank, B. H., and Veros, A. J. (1968) Physical studies on proinsulin-association behavior and conformation in solution. *BBRC* **32,** 155–160
45. Kuliawat, R., and Arvan, P. (1994) Distinct molecular mechanisms for protein sorting within immature secretory granules of pancreatic β-cells. *J. Cell Biol.* **126,** 77–86
46. Malide, D., Seidah, N. G., Chrétien, M., and Bendayan, M. (1995) Electron microscopic immunocytochemical evidence for the involvement of the convertases PC1 and PC2 in the processing of proinsulin in pancreatic β-cells. *J. Histochem. Cytochem.* **43,** 11–19
47. Zhu, X., Orci, L., Carroll, R., Norrbom, C., Ravazzola, M., and Steiner, D. F. (2002) Severe block in processing of proinsulin to insulin accompanied by elevation of des-64,65 proinsulin intermediates in islets of mice lacking prohormone convertase 1/3. *Proc. Natl. Acad. Sci. U.S.A.* **99,** 10299–10304
48. Roth, J., Kasper, M., Stamm, B., Häcki, W. H., Storch, M. J., Madsen, O. D., Klöppel, G., and Heitz, P. U. (1989) Localization of proinsulin and insulin in human insulinoma. Preliminary immunohistochemical results. *Virchows Arch. B Cell Pathol. Incl. Mol. Pathol.* **56,** 287–292
49. Sempoux, C., Guiot, Y., Dubois, D., Moulin, P., and Rahier, J. (2001) Human type 2 diabetes. Morphological evidence for abnormal β-cell function. *Diabetes* **50,** S172-S177
50. Zhu, Y. L., Abdo, A., Gesmonde, J. F., Zawalich, K. C., Zawalich, W., and Dannies, P. S. (2004) Aggregation and lack of secretion of most newly synthesized proinsulin in non-β-cell lines. *Endocrinology* **145,** 3840–3849
51. Orci, L., Ravazzola, M., and Perrelet, A. (1984) (Pro)insulin associates with Golgi membranes of pancreatic B cells. *Proc. Natl. Acad. Sci. U.S.A.* **81,** 6743–6746
52. Orci, L., Ravazzola, M., Amherdt, M., Madsen, O., Perrelet, A., Vassalli, J.-D., and Anderson, R. G. (1986) Conversion of proinsulin to insulin occurs coordinately with acidification of maturing secretory vesicles. *J. Cell Biol.* **103,** 2273–2281
53. Nicolson, T. J., Bellomo, E. A., Wijesekara, N., Loder, M. K., Baldwin, J. M., Gyulkhandanyan, A. V., Koshkin, V., Tarasov, A. I., Carzaniga, R., Kronenberger, K., Taneja, T. K., da Silva Xavier, G., Libert, S., Froguel, P., Scharfmann, R., Stetsyuk, V., Ravassard, P., Parker, H., Gribble, F. M., Reimann, F., Sladek, R., Hughes, S. J., Johnson, P. R., Masseboeuf, M., Burcelin, R., Baldwin, S. A., Liu, M., Lara-Lemus, R., Arvan, P., Schuit, F. C., Wheeler, M. B., Chimienti, F., and Rutter, G. A. (2009) Insulin storage and glucose homeostasis in mice null for the granule zinc transporter ZnT8 and studies of the type 2 diabetes-associated variants. *Diabetes* **58,** 2070–2083
54. Liu, M., Haataja, L., Wright, J., Wickramasinghe, N. P., Hua, Q. X., Phillips, N. F., Barbetti, F., Weiss, M. A., and Arvan, P. (2010) Mutant INS-gene induced diabetes of youth. Proinsulin cysteine residues impose dominant-negative inhibition on wild-type proinsulin transport. *PLoS ONE* **5,** e13333
55. Nakamura, N., Lowe, M., Levine, T. P., Rabouille, C., and Warren, G. (1997) The vesicle docking protein p115 binds GM130, a cis-Golgi matrix protein, in a mitotically regulated manner. *Cell* **89,** 445–455